J. Fluid Mech. (2006), *vol.* 548, *pp.* 361–373.
doi:10.1017/S0022112005007639 Printed in the United Kingdom

Effect of different thermal wall boundary conditions on compressible turbulent channel flow at $M = 1.5$

By S. TAMANO AND Y. MORINISHI

Graduate School of Engineering, Nagoya Institute of Technology, Gokiso-cho, Showa-ku, Nagoya-shi, Aichi-ken 466-8555, Japan

(Received 30 November 2004 and in revised form 1 August 2005)

The main objective of this study is to clarify the effect of thermal wall boundary conditions on turbulence statistics and structures in a compressible turbulent flow. This work is an extension of Morinishi *et al.* (*J. Fluid Mech.* vol. 502, 2004, p. 273), who performed DNS of compressible turbulent channel flow between adiabatic and isothermal walls at Mach number $M = 1.5$ (Case 2). We address the question of whether the modification of turbulence statistics is attributable to the effect of the adiabatic wall boundary condition or the effect of the increase of wall temperature caused by the adiabatic wall boundary condition. New DNS of the compressible turbulent channel flow between isothermal walls with the wall temperature difference at the Mach number $M = 1.5$ (Case 1) and DNS of the corresponding incompressible turbulent flow with passive scalar transport (Case I) are performed. The present study shows that the mean temperature profile near the high-temperature wall for Case 1 has an additional maximum due to the friction work, while such an additional maximum does not appear for Cases 2 and I. The additional maximum leads to a corresponding near-wall maximum of temperature fluctuations. We find the direction of energy transfer due to pressure work near the adiabatic wall for Case 2 being opposite to that near the isothermal wall to be due to the effect of the high-temperature wall, not to the effect of the adiabatic wall. These findings are explained by using the budgets of internal energy and temperature variance transport equations.

1. Introduction

Experimental results on wall-bounded compressible turbulent flow have been discussed and reviewed by Bradshaw (1977), Fernholz & Finley (1977), Lele (1994), Spina, Smits & Robinson (1994) and Smits & Dussauge (1996). These valuable investigations reveal considerable knowledge about the effect of compressibility on, for example, the friction coefficient and the mean velocity profile, which has contributed to the engineering and industrial developments of supersonic vehicles and combustion. For wall-bounded compressible turbulent flow, even if the Mach number is not large, the variation in the temperature profile is usually large near the wall and results in the modification of turbulence statistics and structures, compared to those found in the incompressible counterpart. These modifications are strongly affected by the different thermal wall boundary conditions. However, experimental measurements of temperature and pressure profiles are difficult for wall-bounded compressible turbulent flow, and to the best of our knowledge the effects of the thermal wall boundary conditions on turbulence statistics and structures have not been examined.

As an alternative to experimental investigations of wall-bounded compressible turbulence, direct numerical simulation (DNS) has been used. Coleman, Kim & Moser (1995), Lechner, Sesterhenn & Friedrich (2001) and Foysi, Sarkar & Friedrich (2004) performed DNS of compressible turbulent channel flow between isothermal walls without any wall temperature difference at bulk Mach numbers $M = 3.0$, 1.5 and 3.5. Also, Guarini *et al.* (2000) conducted DNS of the compressible turbulent boundary layer flow on an adiabatic wall with free-stream Mach numbers up to 2.5. To complement these studies, Morinishi, Tamano & Nakabayashi (2004) performed DNS of compressible turbulent channel flow between adiabatic and isothermal walls at $M = 1.5$, and reported differences in turbulence statistics and energy transfer near both the adiabatic and isothermal walls. However, it was not possible to distinguish between the effect of the adiabatic wall boundary condition (i.e. $\partial T/\partial y = 0$) and the effect of the increase of wall temperature caused by the adiabatic wall boundary condition.

As typical numerical simulations with high-temperature wall boundary conditions, Nicoud (1999) and Wang & Pletcher (1996) performed DNS and LES respectively of turbulent channel flow with variable properties between isothermal walls, and investigated the effect of the thermal wall boundary condition on turbulence statistics. However, since the friction work term in the energy transport equation was negligible in their numerical simulations, which corresponds to simulations at zero Mach number, the effect of the high-temperature wall for wall-bounded compressible turbulent flow has not been clarified.

In this study, a new DNS of compressible turbulent channel flow at $M = 1.5$ between isothermal walls with different wall temperatures (Case 1) is performed. DNS of the corresponding incompressible turbulent channel flow with passive scalar transport (Case I) is also performed to compare turbulence statistics between wall-bounded compressible and incompressible turbulent flows with a wall temperature difference. In addition, the DNS data of Case 1 are compared with the DNS data of Morinishi *et al.* (2004) for the compressible turbulent channel flow between adiabatic and isothermal walls at $M = 1.5$ (Case 2), in order to distinguish the effects of the adiabatic wall and the high-temperature wall on turbulence statistics and structures. In addition to the effect of the different thermal wall boundary conditions, the effect of the Mach number is important for wall-bounded compressible turbulent flow. Readers are referred to the study of Foysi *et al.* (2004) in which the effect of the Mach number on the turbulence statistics for compressible turbulent channel flow between isothermal walls is thoroughly examined using DNS data up to $M = 3.5$.

2. Details of the DNS

2.1. *Numerical methods*

The continuity, momentum and internal energy equations are solved in the DNS of compressible turbulent channel flow. We use the DNS algorithm presented by Morinishi, Tamano & Nakabayashi (2003), which is based on an eighth-order B-spline collocation method in the wall-normal (x_2) direction and the Fourier Galerkin method in the streamwise and spanwise (x_1, x_3) directions, and a third-order low-storage Runge–Kutta time-advancement scheme. The validity of the present code was proven by comparing our results with those of an existing DNS of Coleman *et al.* (1995) (see Morinishi *et al.* 2003).

For incompressible turbulent channel flow with passive scalar transport, the continuity, Navier–Stokes and passive scalar transport equations are solved by a DNS

Case	Re	Re_τ	M	Pr	γ	$L_1 \times L_2 \times L_3$	$N_1 \times N_2 \times N_3$
1	3000	(104–267)	1.5	0.72	1.4	$4\pi H \times 2H \times 4\pi H/3$	$120 \times 240 \times 120$
2	3000	(86.4–279)	1.5	0.72	1.4	$4\pi H \times 2H \times 4\pi H/3$	$120 \times 240 \times 120$
I	(2291)	150	—	0.72	—	$4\pi H \times 2H \times 4\pi H/3$	$128 \times 129 \times 128$

TABLE 1. Physical and numerical simulation parameters.

algorithm which consists of the Chebyshev-tau method in the x_2-direction and the Fourier Galerkin method in the x_1, x_3 directions (see Kleiser & Schumann 1980; Werne 1995). A mixed-time-marching method is used, in which the diffusion term is treated implicitly with the Crank–Nicolson method, and the third-order Runge–Kutta method is used for all other terms. The validity of the present incompressible code with passive scalar transport was confirmed by comparing our results with the DNS database of Kasagi & Iida (1999) for incompressible turbulent channel flow with a wall temperature difference.

2.2. *Numerical conditions*

The non-dimensional parameters for the present simulations of compressible turbulent channel flows (Cases 1 and 2) are the Reynolds number $Re = 3000$, the Mach number $M = 1.5$, the Prandtl number $Pr = \mu c_p/\kappa = 0.72$, and the ratio of specific heats $\gamma = c_p/c_v = 1.4$ (where κ is thermal conductivity, μ is molecular viscosity, c_p is specific heat at constant pressure, and c_v is specific heat at constant volume). In this paper, ρ and T are the density and temperature, respectively. The Reynolds number, $Re = \rho_m U_m H/\mu_{lw}$, is based on the bulk density, bulk velocity, channel half-width, and viscosity at the lower wall, and the Mach number, $M = U_m/(\gamma R T_{lw})^{1/2}$ (where $R = (\gamma - 1)c_p/\gamma$ is the gas constant), is based on the bulk velocity and sound speed at the lower wall, where the subscript lw denotes the Reynolds-averaged value at the lower wall. On the other hand, the non-dimensional parameters for the present simulations of incompressible turbulent channel flow with passive scalar transport (Case I) are the Reynolds number $Re_\tau = 150$ and the Prandtl number $Pr = 0.72$. The Reynolds number, $Re_\tau = u_\tau H/\nu$, is based on the friction velocity, the channel half-width, and the kinematic viscosity. Note that the Reynolds number Re_τ for the compressible turbulent flow is given by $Re_\tau = H/\delta_v$, where $\delta_v = \mu_w/(\rho_w u_\tau)$, $u_\tau = (\tau_w/\rho_w)^{1/2}$, and τ_w are the viscous length scale, the friction velocity, and the wall shear stress, respectively. The physical and numerical parameters for all cases are given in table 1. (N_1, N_2, N_3) and (L_1, L_2, L_3) are the number of grid points and computational region in the x_1-, x_2- and x_3-directions, respectively.

The no-slip wall boundary condition for the three velocity components is used for all cases. The upper and lower walls of Case 1 are isothermal with the wall temperature difference ΔT_w, where the upper wall temperature is higher than the lower, while the upper and lower walls of Case 2 are adiabatic and isothermal, respectively. The wall boundary condition of Case I corresponds to that of Case 1. To classify the computational cases corresponding to thermal wall boundary conditions, Cases 1L, 1H, 2I and 2A are introduced for the compressible turbulent flow, where Cases 1L and 1H represent the low- and high-temperature wall sides of Case 1, respectively, and Cases 2I and 2A represent the isothermal and adiabatic wall sides of Case 2, respectively.

For compressible turbulent channel flow, the grid resolution is evaluated by using not only the Reynolds number based on the viscous length scale, Re_τ, but also the Reynolds number based on the semi-local viscous length scale, $Re_\tau^* = H/\delta_{v*}$, where

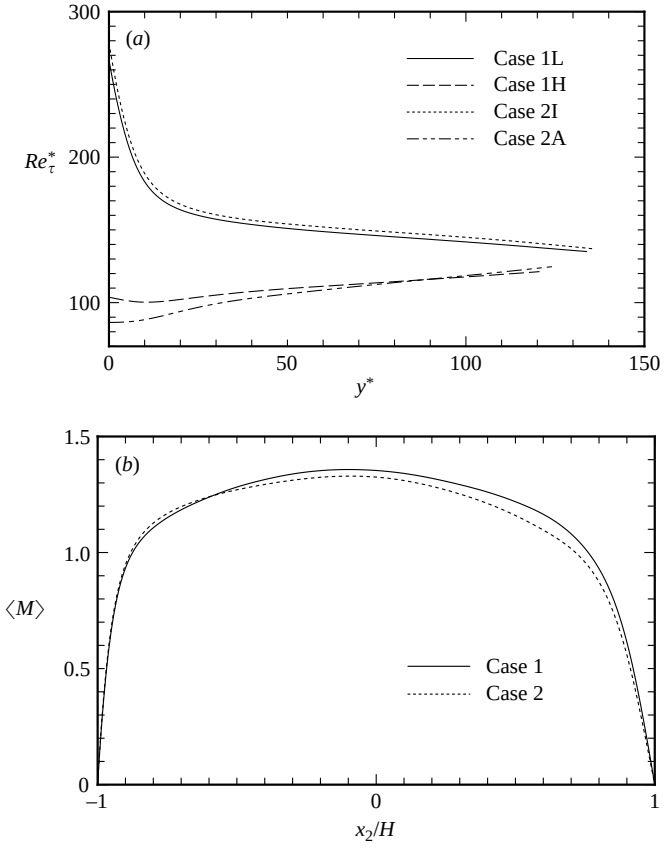

FIGURE 1. (*a*) Semi-local friction Reynolds number. (*b*) Local mean Mach number.

Case	Δx_1^+	Δx_2^+	Δx_3^+	Δx_1^*	Δx_2^*	Δx_3^*
1L	28	0.33–4.6	9.3	14–28	0.33–2.3	4.7–9.3
1H	11	0.13–1.8	3.6	11–13	0.13–2.1	3.6–4.2
2I	29	0.35–4.8	9.7	14–29	0.35–2.4	4.8–9.7
2A	9.1	0.11–1.5	3.0	9.1–13	0.11–2.2	3.0–4.4
I	15	0.045–3.7	4.9	15	0.045–3.7	4.9

TABLE 2. Grid resolution.

$\delta_{v*} = \langle\mu\rangle/(\langle\rho\rangle u_{\tau*})$ and $u_{\tau*} = (\tau_w/\langle\rho\rangle)^{1/2}$ are the semi-local viscous length scale and semi-local friction velocity, respectively. Here, $\langle\ \rangle$ represents the Reynolds average over time and the x_1- and x_3-directions. The profile of Re^*_τ is shown in figure 1(*a*). The semi-local wall unit $y^* = y/\delta_{v*}$ is used in the figure, instead of the usual wall unit $y^+ = y/\delta_v$, where y is the distance from the wall. Figure 1(*a*) shows that the profiles of Re^*_τ for Cases 1L and 1H almost agree with those for Cases 2I and 2A, respectively. Note that $u_{\tau*}$, δ_{v*} and y^* correspond to u_τ, δ_v and y^+, respectively, for incompressible turbulent channel flow (Case I), due to the constant fluid properties.

Grid resolution based on wall and local variables for the present simulations is shown in table 2. The grid resolution in the wall unit and semi-local wall

unit is evaluated by using $\Delta x_i^+ = \Delta x_i/\delta_v$ and $\Delta x_i^* = \Delta x_i/\delta_{v*}$, respectively, where $\Delta x_i (i = 1, 2, 3)$ is the grid width in the x_i-direction. The resolution of Cases 1 and 2 is comparable with that of Coleman *et al.* (1995) and Guarini *et al.* (2000) for compressible turbulent flow, while the resolution of Case I is comparable with that of Kasagi & Iida (1999) for incompressible turbulent flow. In addition, we confirmed that the present DNS data had sufficient resolution and domain size by examining one-dimensional energy spectra and two-point correlations.

Although the semi-local friction Reynolds number is similar for Cases 1 and 2, special care should be taken regarding the Mach number effect, especially in comparing with Case I (incompressible flow), since a semi-local scaling cannot account for both Mach and Reynolds number effects. The profile of local mean Mach number $\langle M \rangle = \langle u_1 \rangle / (\gamma R \langle T \rangle)^{1/2}$ is given in figure 1(*b*). It is seen that the profiles of $\langle M \rangle$ for Cases 1 and 2 are similar to each other, and they are greater than unity except near the wall. Their maxima are about 1.3 which is smaller than maximum ($\simeq 2.3$) of Foysi *et al.* (2004) at $M = 3.5$, but the present compressible situations are adequate for supersonic channel flows.

3. Results and discussion

3.1. *Profiles of mean temperature and root-mean-square temperature fluctuation*

The profile of mean temperature $(\langle T \rangle - T_{lw})/\Delta T_w$ is shown in figure 2(*a*), where ΔT_w is the difference in temperature at the upper and lower walls. The profile of mean temperature for Case I is antisymmetric with respect to the location $x_2/H = 0$, while it is not for Cases 1 and 2. The mean temperature gradients near the centre of the channel for all cases are almost the same. The figure shows that the maximum of the mean temperature appears near the high-temperature wall for Case 1, while it does not appear near the high-temperature wall for Case I because friction work does not exist for incompressible turbulent flow with passive scalar transport. This is supported by the finding that the temperature profile near the wall simulated by Nicoud (1999) for $M \simeq 0$ agrees well with that of Case I and is significantly different from that of Case 1. The mean temperature of Case 2 approaches the upper wall with zero slope, owing to the adiabatic wall boundary condition. The difference in the mean temperature profiles of Cases 1 and 2 near the upper wall is explained by examining the budget of the internal energy transport equation (see § 3.2).

Figure 2(*b*) shows the profile of root-mean-square (RMS) temperature fluctuation $(T')_{rms}/\Delta T_w = \sqrt{\langle T'^2 \rangle}\ /\Delta T_w$, where the prime represents the turbulent fluctuation with respect to the Reynolds average $\langle\ \rangle$. The maximum of $(T')_{rms}/\Delta T_w$ appears at the centre of the channel for Case I, while it appears near the lower and upper walls for Cases 1 and 2, respectively. The peaks of $(T')_{rms}/\Delta T_w$ near the lower wall for Cases 1 and 2 are totally different. The profile of $(T')_{rms}/\Delta T_w$ for Case 1 has an additional maximum in the region very close to the high-temperature (upper) wall. This maximum for Case 1 is produced by the maximum of the mean temperature near the high-temperature wall; this mechanism is explained by examining the budget of the temperature variance transport equation (see § 3.3).

3.2. *Budget of internal energy*

For compressible turbulent channel flow, energy is transferred among the turbulent kinetic, mean kinetic and internal energy components, while their total remains fixed. Here, we focus on the transport equation of the internal energy $\{e\} = c_v\{T\}$ to better understand the mean temperature profiles with different thermal wall boundary

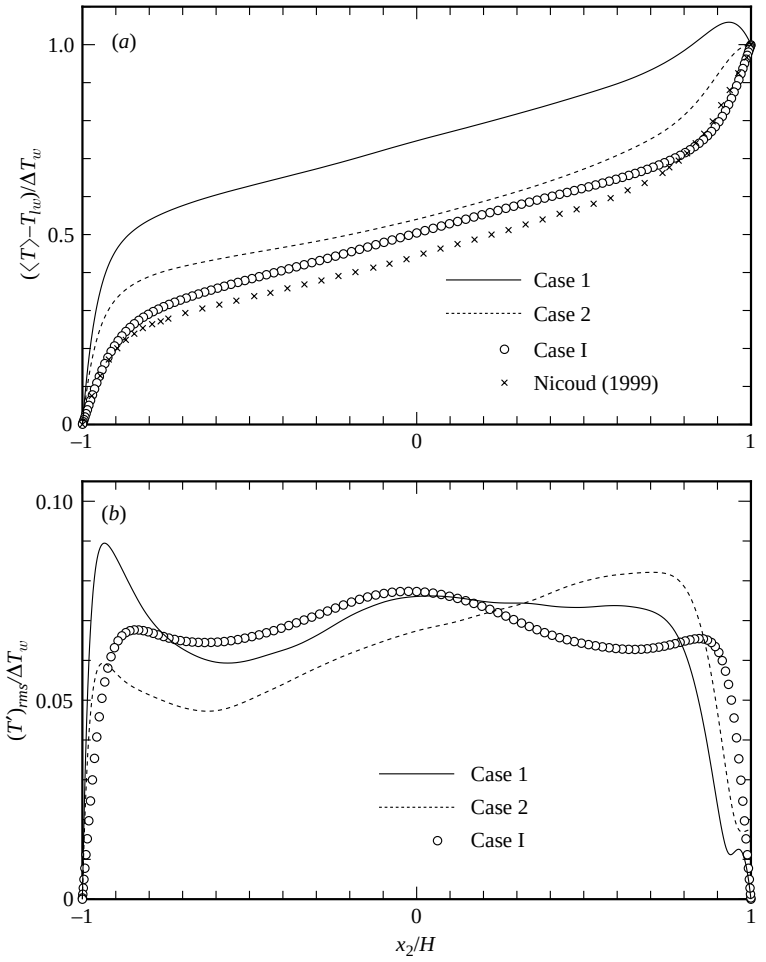

FIGURE 2. (*a*) Mean temperature. (*b*) RMS temperature fluctuation.

conditions. In this paper, the Favre average of a quantity ϕ is given by $\{\phi\} = \langle\rho\phi\rangle/\langle\rho\rangle$, and a double prime represents the turbulent fluctuation with respect to the Favre average. The internal energy equation in fully developed turbulent channel flow is as follows (see Huang, Coleman & Bradshaw 1995; Morinishi *et al.* 2004):

$$D_{e1} + D_{e2} + \varepsilon_{vK} + \varepsilon_{\mathrm{k}} - C_{K1} - C_{\mathrm{k}3} = 0, \tag{3.1}$$

where $D_{e1} = -\partial(\langle\rho\rangle c_v\{u_2''T''\})/\partial x_2$ is the turbulent diffusion term, $D_{e2} = -\partial\langle q_2\rangle/\partial x_2$ is the molecular diffusion term ($q_j = -\kappa\partial T/\partial x_j$ is heat flux), $\varepsilon_{vK} = \langle\tau_{i2}\rangle\partial\langle u_i\rangle/\partial x_2$ is the viscous dissipation per unit volume, $\varepsilon_{\mathrm{k}} = \langle\tau'_{ij}\partial u'_i/\partial x_j\rangle$ is the dissipation per unit volume, $C_{K1} = \langle p\rangle\partial\langle u_2\rangle/\partial x_2$ is the pressure work term, and $C_{\mathrm{k}3} = \langle p'\partial u'_k/\partial x_k\rangle$ is the pressure–dilatation correlation term, where the summation convention applies to the italic indices i, j, k. The profiles of these terms in the internal energy equation for Case 1, scaled by the bulk variable $\rho_m U_m^3/H$, are presented in figure 3. For Case 1, the absolute values of D_{e1}, D_{e2} and ε_{vK} near the lower wall, which corresponds to the low-temperature wall, are larger than those near the upper high-temperature wall. The budgets scaled by the mixture of local and semi-local variables, $\langle\rho\rangle u_{\tau*}^3/\delta_{v*}$, for Cases 1L and 1H are shown in figures 4(*a*) and 4(*b*), respectively. The absolute

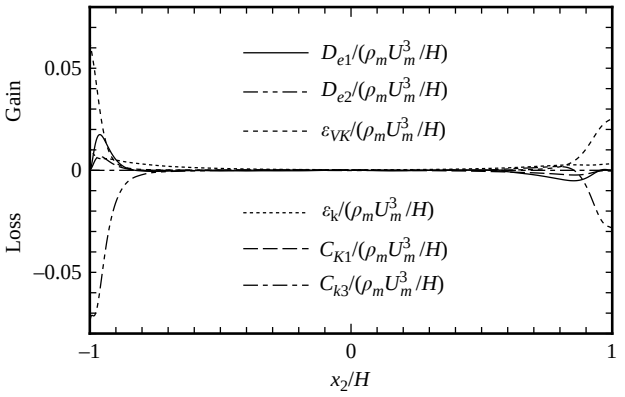

FIGURE 3. Budgets of internal energy transport equation for Case 1.

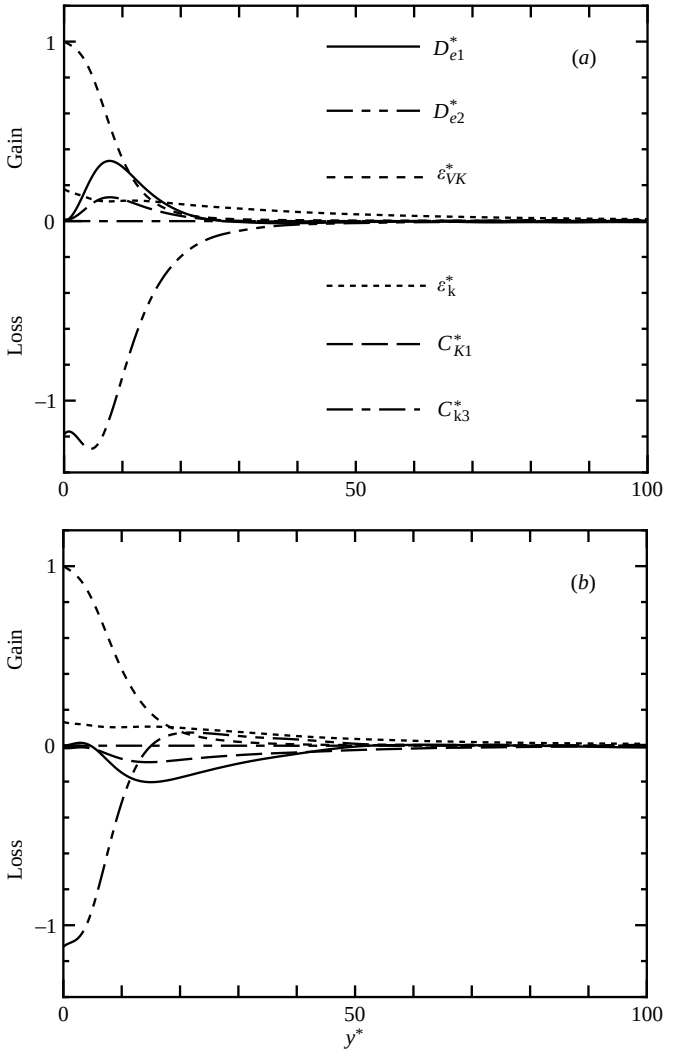

FIGURE 4. Internal energy budgets in semi-local wall units: (*a*) Case 1L and (*b*) Case 1H.

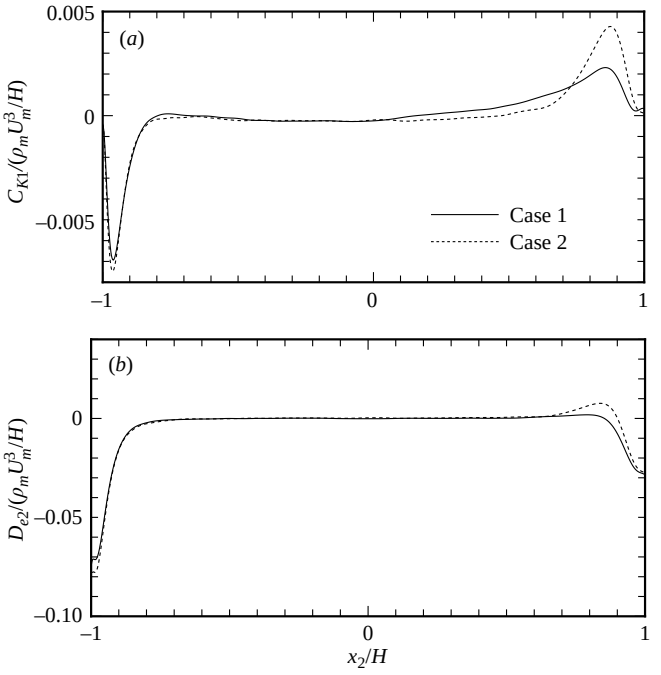

FIGURE 5. (*a*) Pressure work term. (*b*) Molecular diffusion term.

values of D_{e1}^*, D_{e2}^* and $\varepsilon_{\nu K}^*$ for Case 1L are comparable with those for Case 1H, which indicates that the difference observed in the internal energy budget scaled by $\rho_m U_m^3/H$ between Cases 1L and 1H is mainly due to the variable property effect. The trend here is the same as that for Case 2 (Morinishi *et al.* 2004). The pressure–dilatation correlation term C_{k3} in figure 3 is almost zero in the present simulation at $M = 1.5$. Hence, we shall examine the pressure work term C_{K1} and molecular diffusion term D_{e2} below.

Figure 5(*a*) shows the profile of the pressure work term C_{K1} for Cases 1 and 2. This term, which is identically zero for the incompressible case, transfers energy between the internal and mean kinetic energy components (Morinishi *et al.* 2004). It is found that the value of C_{K1} is positive both near the high-temperature wall of Case 1 and near the adiabatic wall of Case 2, while it is negative near the lower isothermal wall for Cases 1 and 2. This means that C_{K1} transfers mean kinetic energy to internal energy near the high-temperature and adiabatic walls, while it transfers internal energy to mean kinetic energy near the lower isothermal walls. Thus the direction of energy transfer due to pressure work near the adiabatic wall for Case 2 (opposite to that near the isothermal wall) is attributable to the effect of the increase in wall temperature caused by the adiabatic wall boundary condition, and not to the effect of the adiabatic wall boundary condition itself.

The profile of the molecular diffusion term D_{e2} for Cases 1 and 2 is shown in figure 5(*b*). Near the upper wall, the positive maximum of D_{e2} appears for Case 2, but not for Case 1. This difference leads to a discrepancy between the mean temperature profiles near the high-temperature wall which corresponds to the upper wall of Case 1 and the adiabatic wall which corresponds to the upper wall of Case 2.

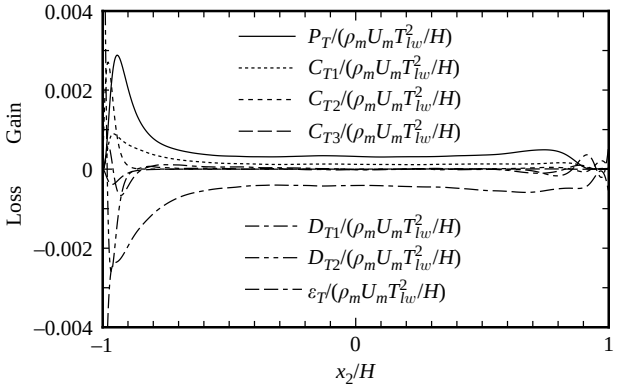

FIGURE 6. Budget of the temperature variance transport equation for Case 1.

3.3. *Budget of temperature variance*

An investigation of the temperature variance budget is helpful for understanding the profile of the RMS turbulent fluctuation. While this has been done for the DNS data from the incompressible passive scalar case, as far as we know it has not for wall-bounded compressible flow. The transport equation of temperature variance $\{T''^2\}$ for fully developed turbulent channel flow is

$$P_T + C_{T1} + C_{T2} + C_{T3} + D_{T1} + D_{T2} - \varepsilon_T = 0, \tag{3.2}$$

where the production term P_T, compressibility terms C_{T1}, C_{T2}, and C_{T3}, turbulent diffusion term D_{T1}, molecular diffusion term D_{T2}, and dissipation per unit volume ε_T are defined as follows:

$$P_T = -\langle\rho\rangle\{T''u_2''\}\partial\{T\}/\partial x_2, \tag{3.3}$$

$$C_{T1} = -\frac{1}{c_v}\left[\langle T''\rangle\langle p\rangle\frac{\partial\langle u_2\rangle}{\partial x_2} + \langle T''\rangle\left\langle p'\frac{\partial u_i'}{\partial x_i}\right\rangle + \langle T'p'\rangle\frac{\partial\langle u_2\rangle}{\partial x_2} + \langle p\rangle\left\langle T'\frac{\partial u_i'}{\partial x_i}\right\rangle\right], \tag{3.4}$$

$$C_{T2} = \frac{1}{c_v}\left[\langle T''\rangle\langle\tau_{i2}\rangle\frac{\partial\langle u_i\rangle}{\partial x_2} + \langle T''\rangle\left\langle\tau_{ij}'\frac{\partial u_i'}{\partial x_j}\right\rangle + \langle T'\tau_{i2}'\rangle\frac{\partial\langle u_i\rangle}{\partial x_2} + \langle\tau_{ij}\rangle\left\langle T'\frac{\partial u_i'}{\partial x_j}\right\rangle\right], \tag{3.5}$$

$$C_{T3} = -\langle T''\rangle\partial\langle q_2\rangle/\partial x_2/c_v, \tag{3.6}$$

$$D_{T1} = -\partial(\langle\rho\rangle\{T''^2u_2''\})/\partial x_2/2, \tag{3.7}$$

$$D_{T2} = \frac{1}{c_v}\frac{\partial}{\partial x_2}\left(\langle T'\kappa'\rangle\frac{\partial\langle T\rangle}{\partial x_2} + \left\langle T'\kappa'\frac{\partial T'}{\partial x_2}\right\rangle + \langle\kappa\rangle\left\langle T'\frac{\partial T'}{\partial x_2}\right\rangle\right), \tag{3.8}$$

$$\varepsilon_T = \frac{1}{c_v}\left[\left\langle\kappa'\frac{\partial T'}{\partial x_2}\right\rangle\frac{\partial\langle T\rangle}{\partial x_2} + \left\langle\kappa'\frac{\partial T'}{\partial x_j}\frac{\partial T'}{\partial x_j}\right\rangle + \langle\kappa\rangle\left\langle\frac{\partial T'}{\partial x_j}\frac{\partial T'}{\partial x_j}\right\rangle\right], \tag{3.9}$$

where the pressure p is evaluated by the state equation. Figure 6 shows these terms in the temperature variance transport equation for Case 1, scaled by $\rho_m U_m T_{lw}^2/H$. The values of the production P_T and dissipation ε_T near the lower wall are larger than those near the upper higher-temperature wall. The contribution of the compressibility terms C_{T1}, C_{T2} and C_{T3} to the energy transfer is not negligible near the lower-temperature wall. Note that these compressibility terms have not been taken into account in the study of turbulent flow with variable properties by Wang & Pletcher (1996). The profiles of the production term P_T for Cases 1 and 2 are shown in figure 7. A weak maximum for Case 1 appears in the region very close to the upper wall, while

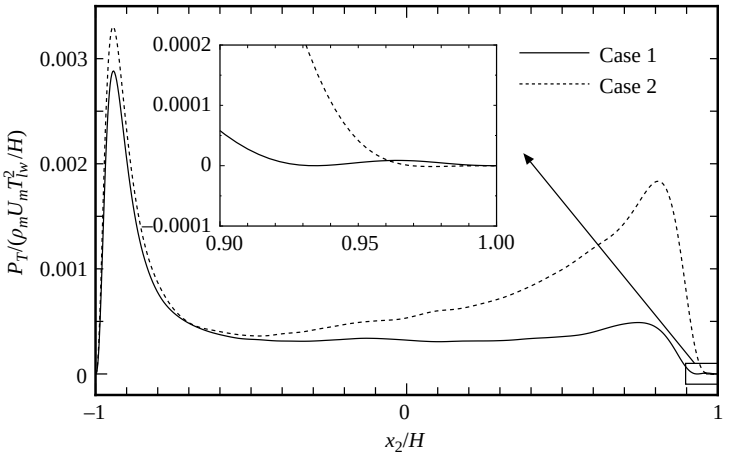

FIGURE 7. Production terms in the temperature variance transport equation.

it is not seen for Case 2. The maximum of P_T for Case 1 corresponds to the maximum of the RMS temperature fluctuation in the region very close to the high-temperature wall.

3.4. *Higher-order statistics*

The higher-order statistics, i.e. the skewness and flatness factors, are useful in understanding the near-wall turbulence structures of wall-bounded turbulent flow. For wall-bounded compressible turbulent flow, however, our knowledge of these quantities remains incomplete (Tamano & Morinishi 2000). The skewness factors of the streamwise and wall-normal velocity fluctuations, $S(u_1') = \langle u_1'^3 \rangle / (u_1')^3_{rms}$ and $S(u_2') = \langle u_2'^3 \rangle / (u_2')^3_{rms}$, are shown in figures 8(*a*) and 8(*b*), respectively. The flatness factors of the streamwise and wall-normal velocity fluctuations, $F(u_1') = \langle u_1'^4 \rangle / (u_1')^4_{rms}$ and $F(u_2') = \langle u_2'^4 \rangle / (u_2')^4_{rms}$, are shown in figures 9(*a*) and 9(*b*), respectively. Note that the semi-local wall unit is used as the abscissa in these figures. The profiles of $S(u_1')$ and $F(u_1')$ for Cases 1 and 2 agree well with the incompressible data (Case I), which do not depend on the thermal boundary conditions. This means that Morkovin's hypothesis, which assumes that the compressibility effect is mainly due to the variable property effect and that the turbulence structures of compressible boundary layers are comparable with those of incompressible ones when the variable property effect is taken into account, is correct for the higher-order turbulence statistics of the streamwise velocity fluctuation (Morkovin 1962). However, the profiles of $S(u_2')$ and $F(u_2')$ for compressible flow do not collapse on the data of Case I in the region $y^* < 20$, where the values of $S(u_2')$ for Cases 1L and 2I are smaller than those for Cases 1H and 2A, while the values of $F(u_2')$ for Cases 1L and 2I are larger. The difference in $S(u_2')$ and $F(u_2')$ between compressible and incompressible flows is due to the low Reynolds number and the effect of compressibility, which correspond to the fact that $\langle u_2'' \rangle = \langle u_2 \rangle - \{u_2\} = -\langle \rho' u_2' \rangle / \langle \rho \rangle$ is not zero due to density fluctuations.

4. Conclusions

To complement the related study of Morinishi *et al.* (2004), where the effect of different thermal wall boundary conditions on turbulence statistics was investigated using DNS of compressible turbulent channel flow between adiabatic and isothermal

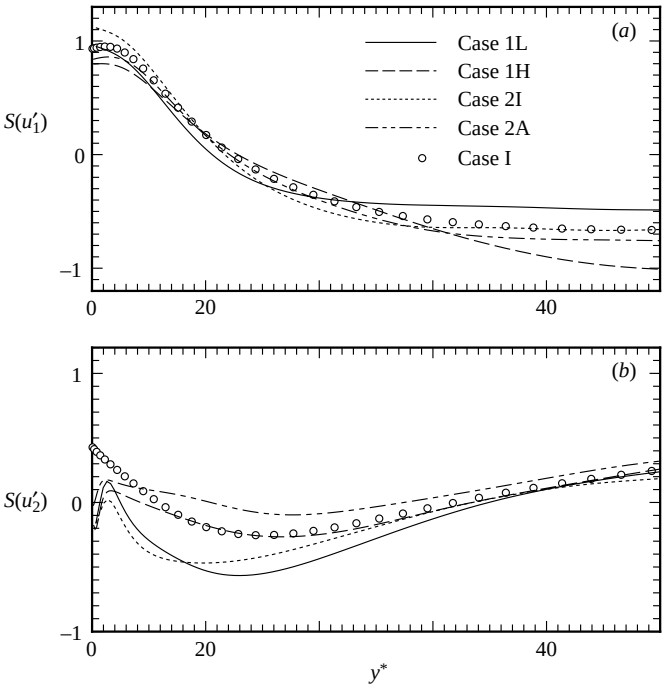

FIGURE 8. Skewness factors: (*a*) $S(u_1')$ and (*b*) $S(u_2')$.

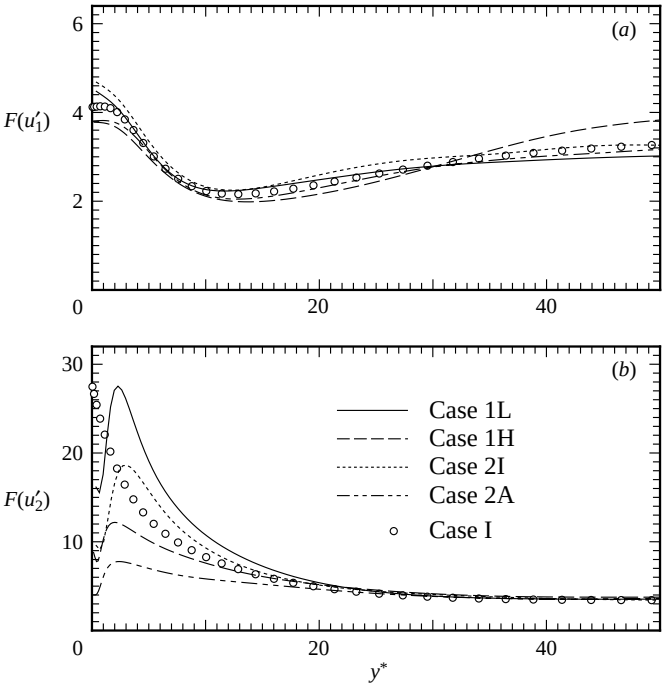

FIGURE 9. Flatness factors: (*a*) $F(u_1')$ and (*b*) $F(u_2')$.

walls at Mach number $M = 1.5$ and $Re = 3000$ (Case 2), DNS of compressible turbulent channel flow between isothermal walls with different temperatures at $M = 1.5$ and $Re = 3000$ (Case 1) and DNS of incompressible turbulent channel flow between isothermal walls with different temperatures at $Re_\tau = 150$ (Case I) were performed. To clarify the difference between the effect of the rise in wall temperature due to the adiabatic wall boundary condition and the effect due to the high-temperature wall boundary condition, DNS data of Cases 1 and 2 were compared with each other.

Near the high-temperature wall for Case 1, the mean temperature profile has an additional maximum due to the friction work, which does not appear for Cases 2 and I. The additional maximum leads to the corresponding maximum of RMS temperature fluctuation. This is consistent with the numerical result that the production term of temperature variance has an additional maximum in the region very close to the high-temperature wall. The difference in the mean temperature profiles at the high-temperature and adiabatic walls is explained by the numerical result that a positive maximum of the molecular diffusion term appears near the upper wall for Case 2, but not for Case 1. The direction of energy transfer due to pressure work near the high-temperature wall for Case 1 is the same as that near the adiabatic wall for Case 2. This explains why the direction of energy transfer due to pressure work near the adiabatic wall for Case 2 being opposite to that near the isothermal wall is attributable to the effect of the high-temperature wall, not to the effect of the adiabatic wall. The compressibility terms of the temperature variance transport equation are not negligible near the low-temperature wall for Case 1.

The computations performed on a FUJITSU VPP5000 at the Center for Promotion of Computational Science and Engineering, Japan Atomic Energy Research Institute, are gratefully acknowledged.

REFERENCES

Bradshaw, P. 1977 Compressible turbulent shear layers. *Annu. Rev. Fluid Mech.* **9**, 33–54.

Coleman, G. N., Kim, J. & Moser, R. D. 1995 A numerical study of turbulent supersonic isothermal-wall channel flow. *J. Fluid Mech.* **305**, 159–183.

Fernholz, H. H. & Finley, P. J. 1977 A critical complication of compressible turbulent boundary layer data. *AGARD-AG* **223**.

Foysi, H., Sarkar, S. & Friedrich, R. 2004 Compressibility effects and turbulence scaling in supersonic channel flow. *J. Fluid Mech.* **509**, 207–216.

Guarini, S. E., Moser, R. D., Shariff, K. & Wray, A. 2000 Direct numerical simulation of a supersonic turbulent boundary layer at Mach 2.5. *J. Fluid Mech.* **414**, 1–33.

Huang, P. G., Coleman, G. N. & Bradshaw, P. 1995 Compressible turbulent channel flows: DNS results and modelling. *J. Fluid Mech.* **305**, 185–218.

Kasagi, N. & Iida, O. 1999 Progress in direct numerical simulation of turbulent heat transfer. *Proc. 5th ASME–JSME Joint Thermal Eng. Conf., San Diego, California, March 15–19*. CD-ROM.

Kleiser, L. & Schumann, U. 1980 Treatment of incompressibility and boundary conditions in 3-D numerical spectral simulations of plane channel flows. *Proc. 3rd GAMM Conference on Numerical Methods in Fluid Mechanics* (ed. E. H. Hirschel), pp. 165–173. Vieweg, Brauschweig.

Lechner, R., Sesterhenn, J. & Friedrich, R. 2001 Turbulent supersonic channel flow. *J. Turbulence* **2**, 1–25.

Lele, K. 1994 Compressibility effects on turbulence. *Annu. Rev. Fluid Mech.* **26**, 211–254.

Morinishi, Y., Tamano, S. & Nakabayashi, K. 2003 A DNS algorithm using B-spline collocation method for compressible turbulent channel flow. *Computers & Fluids* **32**, 751–776.

Morinishi, Y., Tamano, S. & Nakabayashi, K. 2004 Direct numerical simulation of compressible turbulent channel flow between adiabatic and isothermal walls. *J. Fluid Mech.* **502**, 273–308.

Morkovin, M. V. 1962 Effects of compressibility on turbulent flows. In *Mécanique de la Turbulence* (ed. A. Favre), pp. 367–380. CNRS.

Nicoud, F. C. 1999 Numerical study of a channel flow with variable properties. *CTR Annual Research Briefs – 1998, Stanford Univ./NASA Ames*, pp. 289–310.

Smits, A. J. & Dussauge, J. P. 1996 *Turbulent Shear Layers in Supersonic Flow*. American Institute of Physics.

Spina, E. F., Smits, A. J. & Robinson, S. K. 1994 The physics of supersonic turbulent boundary layers. *Annu. Rev. Fluid Mech.* **26**, 287–319.

Tamano, S. & Morinishi, Y. 2002 DNS of wall-bounded compressible turbulent flow. *Proc. 5th JSME–KSME Fluids Eng. Conf., Nagoya, Japan, Novemver 17–21*, pp. 1461–1466. CD-ROM.

Wang, W. P. & Pletcher, R. H. 1996 On the large eddy simulation of a turbulent channel flow with significant heat transfer. *Phys. Fluids* **8**, 3354–3366.

Werne, J. 1995 Incompressibility and no-slip boundaries in the Chebyshev-tau approximation: Correction to Kleiserand Schumann's influence-matrix solution. *J. Comput. Phys.* **120**, 260–265.